Progress In Electromagnetics Research M, Vol. 77, 93–102, 2019

Triple-Band Polarization-Independent Ultrathin Metamaterial Absorber

Hailin Cao[1, 2, *], Meng Shan[2], Tao Chen[1], Jianmei Lei[1], Linhua Yang[3], and Xiaoheng Tan[2]

Abstract—A novel triple-band ultrathin metamaterial absorber (MA) with polarization independence is designed, characterized and realized in this study. The designed absorber consists of three layers. The top metallic patch is patterned in an ultrathin dielectric substrate that is backed with a ground metallic plate. The numerical simulation results show that the presented metamaterial absorber exhibits three distinct absorption peaks of 99.95%, 99.28% and 96.36% under normal incidence at frequencies of 8.115, 11.4 and 15.12 GHz, respectively. Due to its fourfold symmetry, the absorbing properties are independent of the polarization of the incident radiation angle. Moreover, in the cases of TE and TM polarization modes, the proposed absorber displays an outstanding absorption response over a wide range of incident angles up to 60°. The physical mechanism of the absorption performance is explained by investigating the normalized input impedance, surface current and field distributions at three distinct absorption peaks. Furthermore, the presented absorber is practically validated by the excellent agreement observed between the experimental and simulated results. The designed absorber has an ultrathin thickness of 1 mm, which is $0.027\lambda_0$ with respect to the lowest peak absorption frequency, and can be useful for several potential applications, such as electromagnetic compatibility, stealth technology and super lenses.

1. INTRODUCTION

The concept of a metamaterial (MM), which is a kind of composite man-made material, was first proposed in the end of the last century when Veselago first proposed the unprecedented concept of a left-hand material [1]. MMs have shown attractive electromagnetic properties that do not exist in any natural materials. Hence, MMs are applied in various areas, such as negative index of refraction [2, 3], solar cells [4, 5], antennas [6, 7], invisible cloaks [8, 9], graphene [10, 11], terahertz imaging [12–14], and absorbers [15–17]. In Particular, an MM was experimentally demonstrated by Smith [18], who combined a metallic wire array and split-ring resonators according to the research results of Pendry [19, 20]. Thenceforth, the study of MM has garnered considerable attention, with applications ranging from the microwave regime to the visible regime.

Research on absorbers using metamaterial technology started from the demonstration of a Perfect Metamaterial Absorber by Landy et al. in 2008 [15]. Since then, extensive MM absorbers have been achieved and exhibit extraordinary characteristics, such as single-band [21, 22], dual-band [17, 23], multi-band [24–26], broadband [27, 28], polarization-independent [25, 29, 30] and wide oblique incident angle [23, 31, 32]. Compared with conventional absorbers, MM absorbers have many advantages including perfect absorption, ultrathin thickness, low profile, and ease of design and fabrication [33]. An absorber with multiple absorption peaks is of great importance in specific applications. To eliminate reflection efficiency and realize multiband absorption, two methods are commonly used. One method is

Received 6 November 2018, Accepted 11 December 2018, Scheduled 25 December 2018

* Corresponding author: Hailin Cao (hailincao@cqu.edu.cn).

[1] State Key Laboratory of Vehicle NVH and Safety Technology, Chongqing 401120, China. [2] College of Communication, Chongqing University, Chongqing 400044, China. [3] Beijing Institute of Spacecraft Environment Engineering, Beijing 100029, China.

periodically arranging multiple different sizes of unit cells in a plane [34] to allow absorber response at multiple bands; however, this approach leads to the increase in the unit cell size of the overall structure. Another conventional method is vertically stacking metallic layers to build a multilayer absorber [35] that enables multiple absorption peaks. As a result of the multilayer arrangement, the thickness of the proposed absorber structure increases, and technique of fabrication becomes much more difficult. Unfortunately, neither of the aforementioned methods is applicable in miniaturization situations. In addition, other methods are adopted to create multi-band absorption in several works by using different modes of one unit cell resonator, arranging various periodic resonance patterns in a dielectric spacing slab on top of a ground metallic board [24–26]. The absorption efficiency of the MM absorber in [24, 25] was not high enough. Moreover, some additional absorption peaks which will limit its application occurred in the absorption spectra [25]. The absorber in [26] realizing triple-band absorption has a larger unit cell size. The absorber in [29] has a thicker size, and the simulated absorption efficiency of the first resonance frequency at 7.06 GHz was only 78%.

To contribute to the development of multi-band MM absorber, a novel compact ultrathin MM absorber is numerically and experimentally investigated in this paper. Compared with the previous works, the proposed compact absorber has covered almost all the advantages, such as extremely high absorption efficiencies at three distinct frequencies, prefect absorption response spectrum, independent of polarization and remains stable over a wide range of oblique incident radiation angles in the case of both TE and TM modes. In addition, this absorber is with an ultrathin thickness and made by low-cost materials of FR4 and copper. To gain better understanding of the physical absorption mechanism, the surface current and field distributions at three absorption peaks are discussed in detail. Moreover, the proposed absorber is experimentally validated in a microwave anechoic chamber. The absorbing properties result from the interaction of the magnetic and electronic resonances.

2. STRUCTURE AND DESIGN

The proposed absorber structure is depicted in Figs. 1(a) and (b). Fig. 1(a) shows the side view of the whole structure. Fig. 1(b) reveals the geometric parameters of the periodic unit cell from the top view. The designed absorber consists of three sandwich-like layers. The top metallic patch is patterned in an ultrathin dielectric substrate. A ground metallic plane is backed to restrict the transmission of electromagnetic radiation. To guarantee good conductivity, the top and bottom metallic layers are made of copper, with a conductivity of 5.8×10^7 S/m. For easier fabrication, the thickness of both metallic layers is selected as 0.035 mm. The material of the medium dielectric substrate layer is set as low-cost FR4 material, with relative permittivity $\epsilon_r = 4.3$ and loss tangent $\tan\delta = 0.025$. After optimizing the schematic parameters of the unit cell and thickness, the final geometrical dimensions of the proposed absorber are as follows: $a = 11.6$, $h = 1$, $g = 2$, $s = 1.4$, $m = 0.65$, $n = 0.5$, $d = 0.3$, $e = 0.15$, $u = 2.6$, $c = 5.2$, $t = 1$ mm. In particular, the designed metamaterial absorber is ultrathin, with a thickness of 1 mm, which is only $0.027\lambda_0$ with respect to the lowest frequency among three absorption peaks.

Numerical simulation is conducted using CST Microwave Studio, commercial electromagnetic simulation software. The full wave simulation method and finite element method are adopted. The x direction and y direction of the structure are set as unit cell periodic boundary conditions. Incident plane waves with frequency sweeping from 5 GHz to 17 GHz travel along the z direction, where the Floquet port is modeled. Transverse electric (TE) and transverse magnetic (TM) polarization modes represent the electric field parallel to the x-axis and y-axis, respectively.

The mathematical expression to calculate the absorptivity of the proposed absorber is characterized as:

$$A(\omega) = 1 - R(\omega) - T(\omega) \tag{1}$$

where $A(\omega)$ refers to absorptivity; $R(\omega)$ denotes reflection power; and $T(\omega)$ represents transmission power. $T(\omega) \to 0$, because of the existence of the metallic background. Hence, the absorptivity of the whole structure only corresponds to the reflection part:

$$A(\omega) = 1 - R(\omega) \tag{2}$$

The matching degree between the free space impedance and input impedance of the proposed absorber is responsible for reflection power. To eliminate the reflection coefficient and maximize the

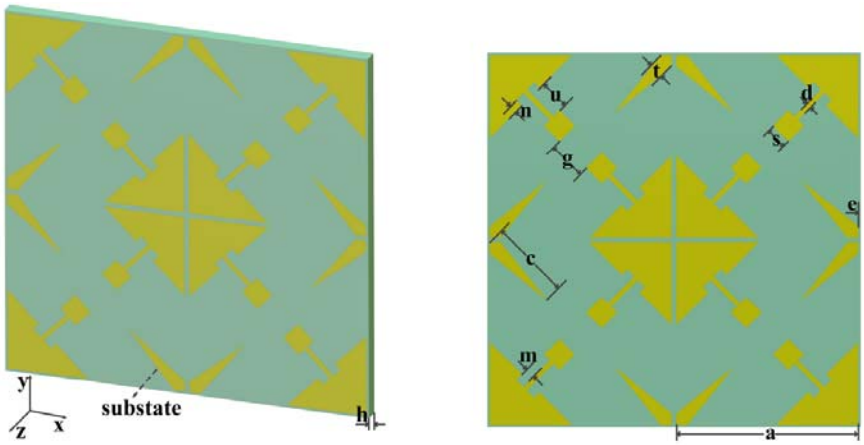

(a) (b)

Figure 1. (a) Side view of the proposed whole structure. (b) Geometric parameters of the periodic unit cell.

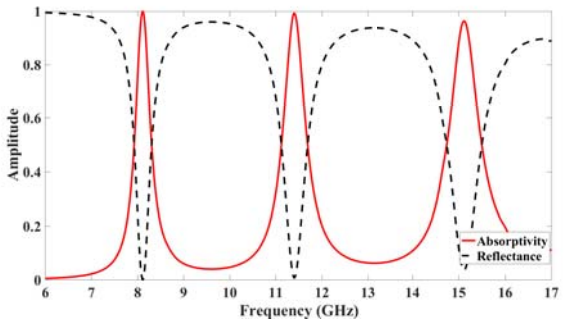

Figure 2. Reflection and absorption performances of the proposed metamaterial absorber.

matching degree, we must optimize the geometric parameter of the unit cell top of patch layer and the overall thickness of the medium dielectric substrate layer.

Figure 2 shows the reflection and absorption performance of the proposed MM absorber when the incident wave is vertically excited. It is shown that there exist three distinct absorption peaks of 99.95%, 99.28% and 96.36% efficiency at frequencies of 8.115 GHz, 11.4 GHz, and 15.12 GHz, respectively. Two absorption peaks lie in X-band and the other in Ku-band. Therefore, this absorber is applicable in certain microwave applications.

3. RESULTS AND ANALYSIS

Under the circumstance of the vertical incidence wave, the reflection coefficient is represented as:

$$S_{11} = -\frac{\eta - \eta_0}{\eta + \eta_0} \tag{3}$$

where η and η_0 represent the structure surface input impedance and free space impedance, respectively. When the maximum match degree between η and η_0 is obtained, i.e., $\eta = \eta_0$, the refection power $R(\omega) = 0$.

According to classical impedance extraction theory [36], the S parameter can be applied to calculate the normalized input impedance of the proposed structure. The normalized input impedance is expressed as:

$$Z = \sqrt{\frac{(1 + S_{11})^2 - S_{21}}{(1 - S_{11})^2 - S_{21}}} \tag{4}$$

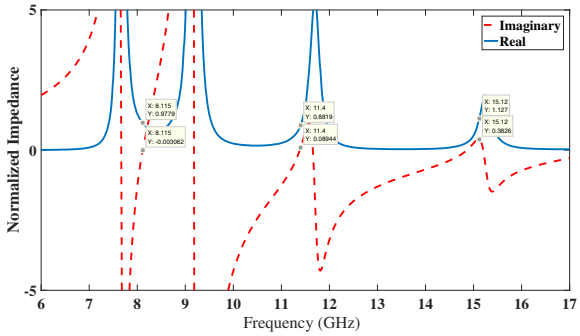

Figure 3. Simulated result of the normalized input impedance of this absorber.

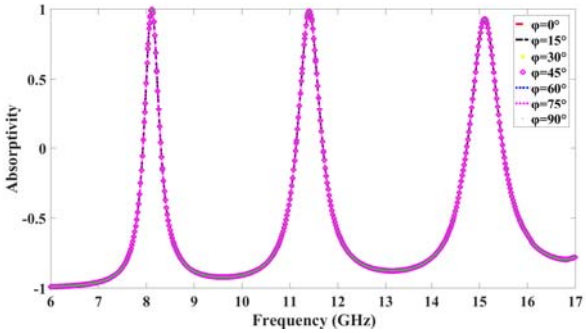

Figure 4. Absorption spectrum of the proposed MM absorber at different incident polarization angles.

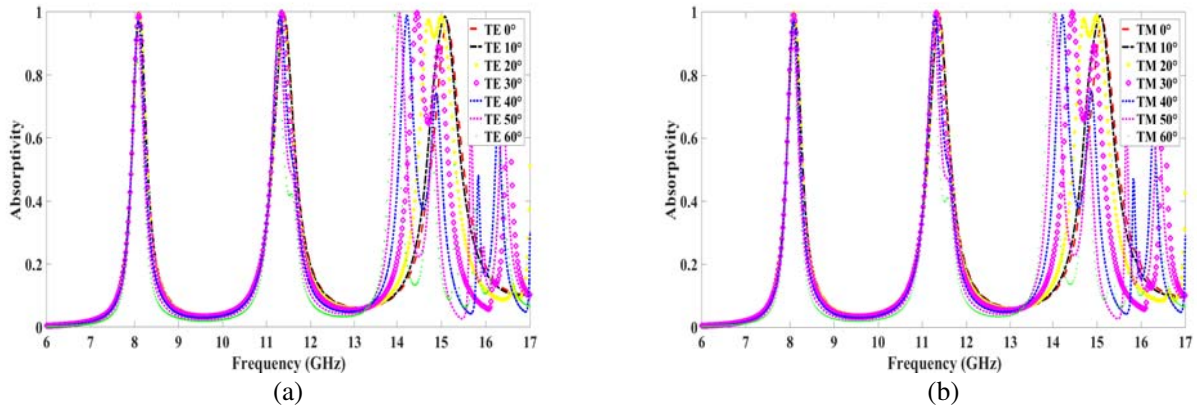

Figure 5. Absorption performance under various oblique incident waves of TE and TM polarization modes: (a) TE; (b) TM.

The plot of normalized input impedance of this absorber is shown in Fig. 3. We can draw the conclusion that, at three distinct absorption peaks, the impedance matching results of the imaginary and real parts are approximately equal to unity and zero, respectively; these results are in good agreement with the simulated results. Moreover, the normalized input impedance further reveals that the proposed structure surface input impedance and free space impedance are well matched.

The absorbing properties under a variety of incident polarization angles are investigated. Up to a 90° polarization angle is considered on account of the fourfold symmetry of the structure. Fig. 4 shows the absorption spectrum of the proposed MM absorber at different incident polarization angles when the incident electromagnetic wave is vertically excited. As shown in Fig. 4, with the polarization angle varying from 0° to 90° in step of 15°, the absorption responses, including the absorption peaks and the corresponding frequencies of this absorber, almost remain unchanged. The simulated results demonstrate that the proposed MM absorber is independent of the polarization angle at normal incidence.

The absorption performances under oblique incident waves of TE and TM polarization modes are studied, as shown in Fig. 5. Fig. 5(a) shows the simulated absorption spectra of various polarization angles of TE mode. In the case of the TE mode, the electric field remains parallel to the x direction, and the propagation direction of magnetic field and incident wave changes with the oblique incident angle. Fig. 5(a) shows that, for incident TE polarization angles ranging from 0° to 30°, the absorptivity at all three distinct frequencies with respect to absorptions peaks remains near unity. Moreover, when the incident polarization angles range from 40° to 60°, the absorptivity at the lowest absorption frequency (8.115 GHz) and the medium absorption frequency (11.4 GHz) decreases as the incident polarization angle increases. Moreover, viewing the absorption response at the highest absorption frequency

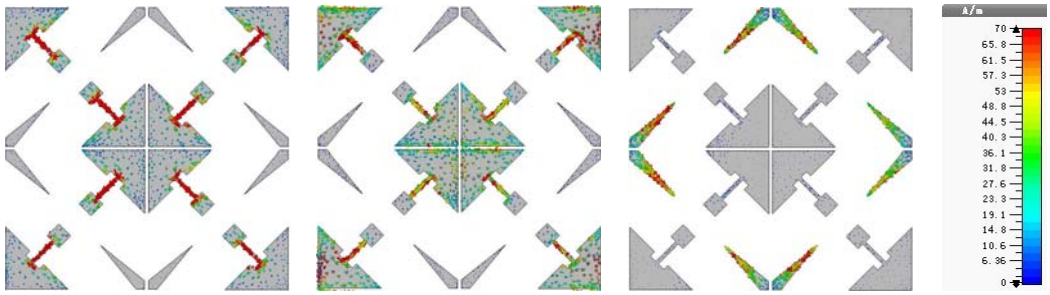

(a) 8.115 GHz (b) 11.4 GHz (c) 15.12 GHz

Figure 6. Current at the top surface.

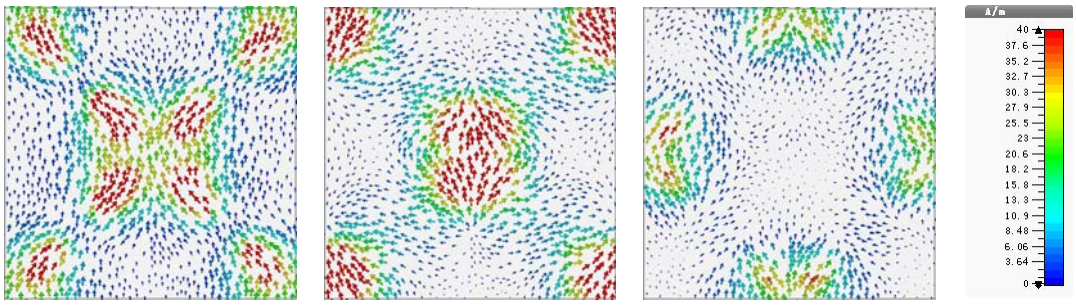

(a) 8.115 GHz (b) 11.4 GHz (c) 15.12 GHz

Figure 7. Current at the bottom surface.

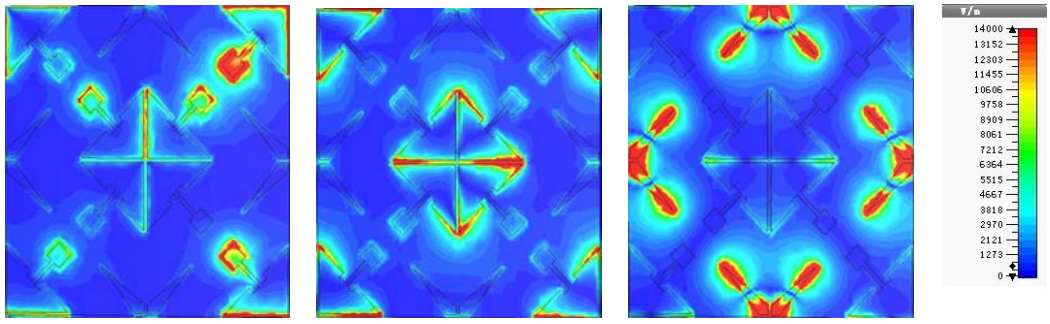

(a) 8.115 GHz (b) 11.4 GHz (c) 15.12 GHz

Figure 8. Electric field.

(15.12 GHz), the highest absorption frequency generally decreases as the incident angle increases, i.e., moves left in Fig. 5(a). Additionally, some other absorption peaks appear at the higher frequency band relative to the highest absorption peak. These additional absorption peaks emerge as a result of the parasitic resonances at the inner proposed structure, and the absorptivity decreases as the incident polarization increases. Fig. 5(b) displays the simulated absorptivity under different polarization angles of the TM mode. Here electric field remains parallel to the y-direction, and the others change with the oblique incident angle. It is clearly seen that the absorption response under TM mode has almost the same trend as that in the case of TE mode.

Furthermore, Fig. 6, Fig. 7, Fig. 8, and Fig. 9 present the resonance characteristics of the current distributions on the top and bottom surfaces as well as the electric field and magnetic field distributions of the proposed absorber at the three bands of 8.115 GHz, 11.4 GHz, and 15.12 GHz, respectively. The surface current direction can be observed from the arrows, and the color refers to the intensity degree.

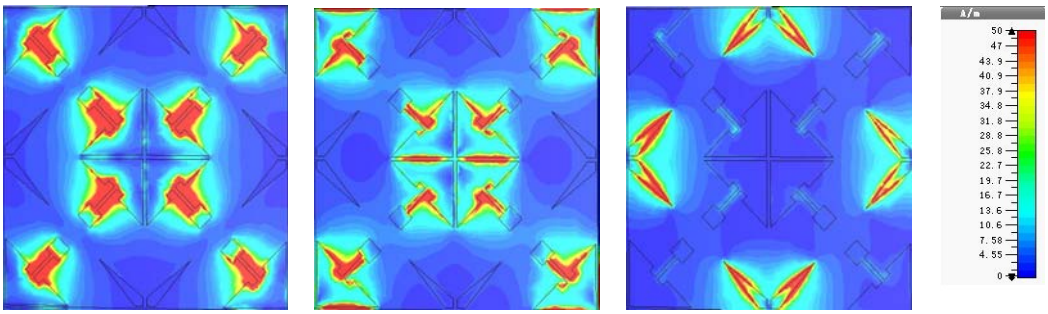

(a) 8.115 GHz (b) 11.4 GHz (c) 15.12 GHz

Figure 9. Magnetic field.

Vertically viewing and comparing Fig. 6(a), Fig. 7(a), Fig. 8(a), and Fig. 9(a), the surface current and the magnetic field distributions at specific frequencies of 8.115 GHz, it is seen that the surface current and magnetic field distributions are in high agreement. The higher surface the current density is, the greater the magnetic field density is, and vice versa. When comparing the surface current and electric field distributions, one can conclude that at the location where the surface current density is enhanced, the magnetic field density is reduced. The same trend is observed at frequencies of 11.4 GHz and 15.12 GHz, as well.

As shown in Fig. 6 and Fig. 7, the surface currents on the top and bottom metal layers of the proposed structure are parallel in opposite directions. This phenomenon indicates that a circulating current loop is formed, and thus magnetic resonances are created at the inner unit cell structure to promote the power loss in the structure. Moreover, the electric dipole response [37] is induced by the coupling between the upper metal layer and the incident electromagnetic waves. It can be clearly identified from the surface current density distributions that, different sections of the metamaterial resonator are responsible for the absorption properties at three discrete resonance frequency bands. The lower and middle absorption resonance frequencies are induced due to the four corners and the center part of the top layer pattern. The higher absorption resonance frequency is attributed to the four sections around midpoint of each edge of the upper layer structure. Hence, the magnetic resonances along with the electric dipole response simultaneously further explain the excellent triple-band absorption performance.

4. EXPERIMENTAL VERIFICATION

The prototype of the proposed ultrathin absorber was fabricated using a standard print circuit board (PCB) technology, as shown in Fig. 10(a). The original fabricated sample with dimensions of 240 mm $\times$ 240 mm is composed of 10×10 unit cell that is printed on an FR-4 dielectric substrate with a thickness of 1 mm, and is backed with a copper layer. For better measurement environment, a larger-scale testing prototype with dimensions of 480 mm $\times$ 480 mm is re-fabricated by combining four original fabricated samples together, and the experimental measurements are conducted in a microwave anechoic chamber. In detail, two broadband standard-gain horn antennas connected to an Agilent E8362C vector network analyzer were used. The block-diagram for practical measurement setup of the presented absorber is depicted in Fig. 10(b). A reference experiment was first performed by measuring the reflectivity of the same-sized copper plate. The actual reflection of the designed absorber was determined by the difference of the reflectivity between the reference copper plate and fabricated prototype.

The experimentally conducted absorptivity of the presented MM absorber at normal incidence compared with the simulated absorptivity is shown in Fig. 11. Clearly, there also exist three distinct absorption frequencies of 8.72, 11.48 and 14.74 GHz, and the corresponding absorption efficiencies are 96.72%, 98.28% and 95.17%, respectively. In comparison, the measured absorption performance has slight deviations in the absorption frequencies and the related absorptivity values. The deviation is caused by factors such as the finite size of the fabricated prototype, the re-fabrication making larger-size testing prototype, and the additional ambient scatters.

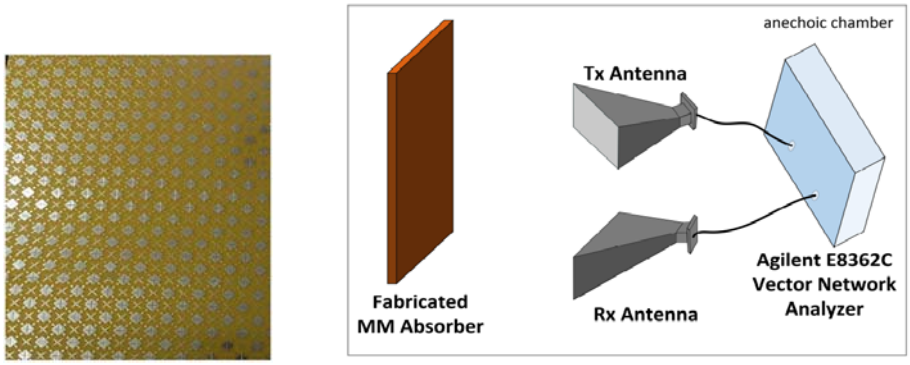

(a) (b)

Figure 10. Experimental varication of the designed structure: (a) Fabricated MM absorber prototype; (b) Block-diagram for practical for Measurement setup.

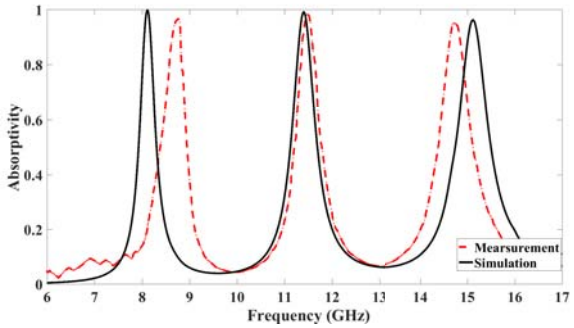

Figure 11. Simulated and measured absorptivity of the proposed metamaterial absorber.

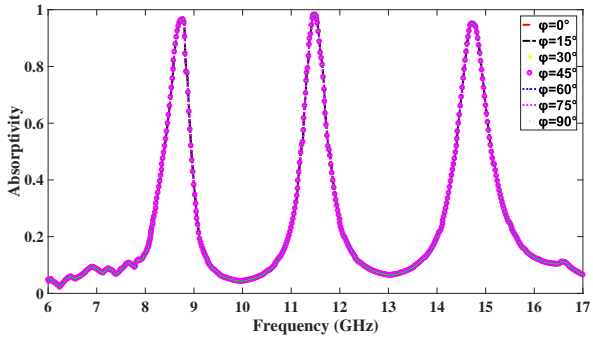

Figure 12. Measured absorptivity of the proposed structure at different incident polarization angles.

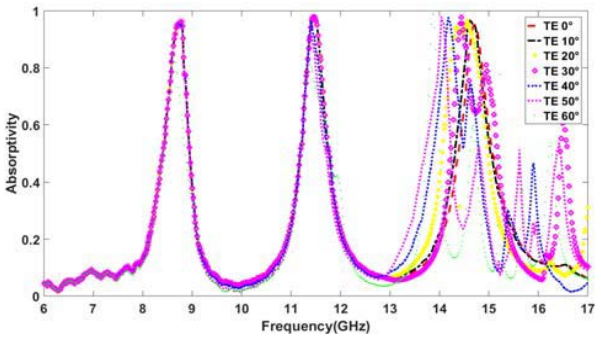

(a)

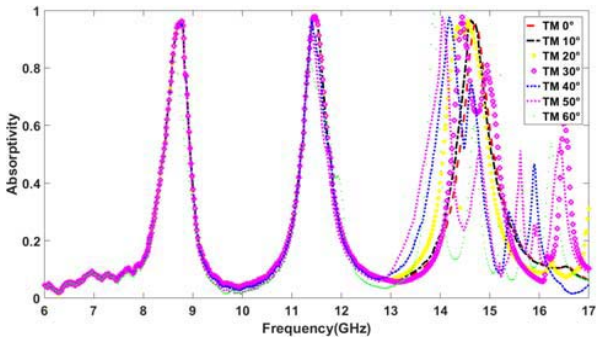

(b)

Figure 13. Measured absorptivity under various oblique incident waves of TE and TM polarization modes: (a) TE; (b) TM.

The absorption spectrum at a variety of polarization angles is experimentally measured, as depicted in Fig. 12. Compared with the simulated absorption spectra, it is obvious that the experimental absorption response is dependent on the polarization angles as well. The three absorption peaks correspondingly float to 8.72, 11.48 and 14.74 GHz, and the absorption efficiencies reduce slightly. From Fig. 13(a) and Fig. 13(b), the measured absorption responses in TE and TM polarization modes with

polarization angles ranging from 0° to 30° verify the high absorption efficiencies of 96.72%, 98.28% and 95.17% at frequencies of 8.72, 11.48 and 14.74 GHz, respectively; these results are in good agreement with the simulated results.

In summary, the measurement results practically verify that the presented metamaterial absorber in this paper is capable of triple-band absorptivity.

5. CONCLUSION

The triple-band polarization-independent metamaterial absorber presented in this paper can realize absorptivities of 99.95%, 99.28% and 96.36% at three distinct absorption frequencies of 8.115 GHz, 11.4 GHz and 15.12 GHz, respectively. Moreover, the proposed absorber was demonstrated to have an ultrathin thickness and exhibited excellent absorption response, regardless of the normal incidence angle, even under a wide range of oblique incident angles. The physical absorption mechanism was investigated by analyzing the surface current and field distribution at the absorption frequencies. The experimental results of the fabricated structure were found in great agreement with the simulated ones. Therefore, the designed absorber can be used in applications such as electromagnetic compatibility, stealth technology, and super lenses.

ACKNOWLEDGMENT

The authors acknowledge the support of the National Natural Science Foundation of China (51877015, 61571069, 51377179, 61301120), the Joint Research Fund in Astronomy (U1831117) under a cooperative agreement between the National Natural Science Foundation of China (NSFC) and the Chinese Academy of Sciences (CAS), the Open Foundation of State Key Laboratory of Vehicle NVH and Safety Technology (Grant No. NVHSKL-201607), the CAST-BISEE Foundation (CAST-BISEE2017-018) and the Open Fund of Guizhou Provincial Key Laboratory of Radio Astronomy and Data Processing (KF201815).

REFERENCES

1. Veselago, V. G., "The electrodynamics of substances with simultaneously negative values of ϵ and μ," *Soviet Physics Uspekhi*, Vol. 10, No. 4, 509–514, 1968.
2. Shalaev, V. M., W. Cai, U. K. Chettiar, H. K. Yuan, A. K. Sarychev, V. P. Drachev, and A. V. Kildishev, "Negative index of refraction in optical metamaterials," *Optics Letters*, Vol. 30, No. 24, 3356–3358, 2005.
3. Zhang, W., J.-Y. Li, and J. Xie, "High sensitivity refractive index sensor based on metamaterial absorber," *Progress In Electromagnetics Research M*, Vol. 71, 107–115, 2018.
4. Liu, Y., Y. Chen, J. Li, T. C. Hung, and J. Li, "Study of energy absorption on solar cell using metamaterials," *Solar Energy*, Vol. 86, No. 5, 1586–1599, 2012.
5. Rufangura, P. and C. Sabah, "Perfect metamaterial absorber for applications in sustainable and high-efficiency solar cells," *Journal of Nanophotonics*, Vol. 12, No. 2, 26002, 2018.
6. Mishra, N. and R. K. Chaudhary, "A miniaturized ZOR antenna with enhanced bandwidth for WiMAX applications," *Microwave and Optical Technology Letters*, Vol. 58, No. 1, 71–75, 2016.
7. Mishra, P. and S. S. Pattnaik, "Metamaterial loaded fractal based interdigital capacitor antenna for communication systems," *Progress In Electromagnetics Research M*, Vol. 70, 127–134, 2018.
8. Chen, H., B. Zheng, L. Shen, H. Wang, X. Zhang, N. I. Zheludev, and B. Zhang, "Ray-optics cloaking devices for large objects in incoherent natural light," *Nature Communications*, Vol. 4, 2652, 2013.
9. Pendry, J. B., D. Schurig, and D. R. Smith, "Controlling electromagnetic fields," *Science*, Vol. 312, 1780–1782, 2006.
10. Lee, S. H., M. Choi, T. T. Kim, S. Lee, M. Liu, X. Yin, and X. Zhang, "Switching terahertz waves with gate-controlled active graphene metamaterials," *Nature Materials*, Vol. 11, No. 1, 936, 2012.

11. Politano, A. and G. Chiarello, "Plasmon modes in graphene: Status and prospect," *Nanoscale*, Vol. 6, No. 19, 10927–10940, 2014.
12. Mitrofanov, O., L. Viti, E. Dardanis, M. C. Giordano, D. Ercolani, A. Politano, and M. S. Vitiello, "Near-field terahertz probes with room-temperature nanodetectors for subwavelength resolution imaging," *Scientific Reports*, Vol. 7, 44240-, 2017.
13. Politano, A., L. Viti, and M. S. Vitiello, "Optoelectronic devices, plasmonics, and photonics with topological insulators," *APL Materials*, Vol. 5, No. 3, 035504, 2017.
14. Yang, Q., J. Gu, D. Wang, X. Zhang, Z. Tian, C. Ouyang, and W. Zhang, "Efficient flat metasurface lens for terahertz imaging," *Optics Express*, Vol. 22, No. 21, 25931–25939, 2014.
15. Landy, N. I., S. Sajuyigbe, J. J. Mock, D. R. Smith, and W. J. Padilla, "Perfect metamaterial absorber," *Physical Review Letters*, Vol. 100, No. 10, 207402, 2008.
16. Yang, C., H. Xiong, and X. P. Li, "Investigation of a metamaterial absorber by using reflection theory model," *Progress In Electromagnetics Research M*, Vol. 59, 65–73, 2017.
17. Ramya, S. and I. Srinivasa Rao, "Design of polarization-insensitive dual band metamaterial absorber," *Progress In Electromagnetics Research M*, Vol. 50, 23–31, 2016.
18. Smith, D. R., W. J. Padilla, and D. C. Vier, "Composite medium with simultaneously negative permeability and permittivity," *Physical Review Letters*, Vol. 84, No. 10, 4184–4187, 2016.
19. Pendry, J. B., A. J. Holden, W. J. Stewart, and I. Youngs, "Extremely low frequency plasmons in metallic mesostructures," *Physical Review Letters*, Vol. 76, No. 25, 4773–4776, 1996.
20. Pendry, J. B., A. J. Holden, D. J. Robbins, and W. J. Stewart, "Member Magnetism from conductors and enhanced nonlinear phenomena," *IEEE Transactions on Microwave Theory and Techniques*, Vol. 47, No. 11, 2075–2084, 1999.
21. Tao, H., C. M. Bingham, A. C. Strikwerda, D. Pilon, D. Shrekenhamer, N. I. Landy, K. Fan, X. Zhang, W. J. Padilla, and R. D. Averitt, "Highly flexible wide angle of incident terahertz metamaterial absorber: Design, fabrication, and characterization," *Physical Review B*, Vol. 78, No. 24, 2008.
22. Ayop, O., M. K. A. Rahim, and N. A. Murad, "Polarization-independent metamaterial absorber for single band and multi-band frequency," *Jurnal Teknologi*, Vol. 77, No. 10, 99–106, 2015.
23. Bagci, F. and F. Medina, "Design of a wide-angle, polarization insensitive,dual-band metamaterial-inspired absorber with the aid ofequivalent circuit model," *Journal of Computational Electronics*, Vol. 16, No. 3, 913–921, 2017.
24. Ayop, O. B., M. K. Abd Rahim, N. A. Murad, N. A. Samsuri, and R. Dewan, "Triple band circular ring-shaped metamaterial absorber for x-band applications," *Progress In Electromagnetics Research M*, Vol. 39, 65–75, 2014.
25. Zhai, H., C. Zhan, Z. Li, and C. Liang, "A triple-band ultrathin metamaterial absorber with wide-angle and polarization stability," *IEEE Antennas and Wireless Propagation Letters*, 241–244, 2015.
26. Bian, B., S. Liu, S. Wang, X. Kong, H. Zhang, B. Ma, and H. Yang, "Novel triple-band polarization-insensitive wide-angle ultra-thin microwave metamaterial absorber," *Journal of Applied Physics*, Vol. 114, No. 10, 194511, 2013.
27. Ling, X., Z. Xiao, X. Zheng, J. Tang, and K. Xu, "Ultra-broadband metamaterial absorber based on the structure of resistive films," *Journal of Electromagnetic Waves and Applications*, Vol. 30, No. 17, 2325–2333, 2017.
28. Shen, G., M. Zhang, Y. Ji, W. Huang, H. Yu, and J. Shi, "Broadband terahertz metamaterial absorber based on simple multi-ring structures," *AIP Advances*, Vol. 8, No. 7, 075206, 2018.
29. Agrawal A., M. Misra, and A. Singh, "Oblique incidence and polarization insensitive multiband metamaterial absorber with quad paired concentric continuous ring resonators," *Progress In Electromagnetics Research M*, Vol. 60, 33–46, 2017.
30. Lu, L., S. Qu, H. Ma, F. Yu, S. Xia, Z. Xu, and P. Bai, "A polarization-independent wide-angle dual directional absorption metamaterial absorber," *Progress In Electromagnetics Research M*, Vol. 27, 91–201, 2012.

31. Agarwal, M., A. K. Behera, and M. K. Meshram, "Wide-angle quad-band polarisation-insensitive metamaterial absorber," *Electronics Letters*, Vol. 52, No. 5, 340–342, 2016.
32. Sood, D. and C. C. Tripathi, "A wideband wide-angle ultra-thin metamaterial microwave absorber," *Progress In Electromagnetics Research M*, Vol. 44, 39–46, 2015.
33. Panaretos, A. H., D. E. Brocker, and D. H. Werner, "Ultra-thin absorbers comprised by cascaded high-impedance and frequency selective surfaces," *IEEE Antennas Wireless Propagation Letters*, Vol. 14, 1089–1092, 2015.
34. Ghosh, S., S. Bhattacharyya, and K. V. Srivastava, "Bandwidth-enhancement of an ultrathin polarization insensitive metamaterial absorber," *Microwave and Optical Technology Letters*, Vol. 56, No. 2, 350–355, 2013.
35. Huang, L. and H. Chen, "Multi-band and polarization insensitive metamaterial absorber," *Progress In Electromagnetics Research*, Vol. 113, 103–110, 2011.
36. Smith, D. R., D. C. Vier, T. Koschny, and C. M., Soukoulis, "Electromagnetic parameter retrieval from inhomogeneous metamaterials," *Physical Review E*, Vol. 71, No. 3, 036617, 2005.
37. Liu, J., Q. Zhou, Y. Shi, X. Zhao, and C. Zhang, "Study of L-shaped resonators at terahertz frequencies," *Applied Physics Letters*, Vol. 103, No. 24, 241911, 2013.